Environment International 126 (2019) 336–345

Contents lists available at ScienceDirect

Environment International

journal homepage: www.elsevier.com/locate/envint

# Green remediation of As and Pb contaminated soil using cement-free clay-based stabilization/solidification

Lei Wang[a,b], Dong-Wan Cho[a,g], Daniel C.W. Tsang[a,*], Xinde Cao[c], Deyi Hou[d], Zhengtao Shen[d,e], Daniel S. Alessi[e], Yong Sik Ok[f], Chi Sun Poon[a]

[a] Department of Civil and Environmental Engineering, The Hong Kong Polytechnic University, Hung Hom, Kowloon, Hong Kong, China
[b] Department of Materials Science and Engineering, The University of Sheffield, Sir Robert Hadfield Building, Mappin St, Sheffield S1 3JD, United Kingdom
[c] School of Environmental Science and Engineering, Shanghai Jiao Tong University, Shanghai 200240, China
[d] School of Environment, Tsinghua University, Beijing 100084, China
[e] Department of Earth and Atmospheric Sciences, University of Alberta, Edmonton T6G 2E3, Canada
[f] Korea Biochar Research Center, O-Jeong Eco-Resilience Institute (OJERI), Division of Environmental Science and Ecological Engineering, Korea University, Seoul 02841, Republic of Korea
[g] Geological Environment Division, Korea Institute of Geoscience and Mineral Resources, Gwahak-ro 124, Yuseong-gu, Daejeon 34132, Republic of Korea

ARTICLE INFO

*Keywords:*
Green/sustainable remediation
Low-carbon contaminant immobilization
Calcined clay
Alkali-activated materials
Waste valorization/recycling
Arsenic/lead leachability

ABSTRACT

Stabilization/solidification (S/S) is a low-cost and high-efficiency remediation method for contaminated soils, however, conventional cement-based S/S method has environmental constraints and sustainability concerns. This study proposes a low-carbon, cement-free, clay-based approach for simultaneous S/S of As and Pb in the contaminated soil, and accordingly elucidates the chemical interactions between alkali-activated clay binders and potentially toxic elements. Quantitative X-ray diffraction and $^{27}Al$ nuclear magnetic resonance analyses indicated that the addition of lime effectively activated the hydration of kaolinite clay, and the presence of limestone further enhanced the polymerization of hydrates. X-ray photoelectron spectroscopy showed that approximately 19% of $As^{[III]}$ was oxidized to $As^{[V]}$ in the alkali-activated clay system, which reduced toxicity and facilitated immobilization of As. During the cement-free S/S process, As and Pb consumed $Ca(OH)_2$ and precipitated as $Ca_3(AsO_4)_2{\cdot}4H_2O$ and $Pb_3(NO_3)(OH)_5$, respectively, accounting for the low leachability of As (7.0%) and Pb (5.4%). However, the reduced amount of $Ca(OH)_2$ decreased the degree of hydration of clay minerals, and the pH buffering capacity of the contaminated soil hindered the pH increase. Sufficient dosage of lime was required for ensuring satisfactory solidification and contaminant immobilization of the clay-based S/S products. The leachability of As and Pb in high-Ca S/S treated soil samples was reduced by 96.2% and 98.8%, respectively. This is the first study developing a green and cement-free S/S of As- and Pb-contaminated soil using clay minerals as an environmentally compatible binding material.

## 1. Introduction

Soil contamination poses serious threats to the sustainability of agroecosystems and global food safety. Potentially toxic elements from contaminated agricultural soil can be acquired and accumulated by edible crops that may pose acute/chronic human health problems (Zhao et al., 2015). Among the toxic elements, chromium (Cr), arsenic (As), cadmium (Cd), mercury (Hg), and lead (Pb) are regarded as priority hazardous contaminants (Tóth et al., 2016; Shi et al., 2017; Huang et al., 2018). Sustainable remediation of contaminated soils containing oxyanionic As and cationic toxic elements such as Pb has been a technical challenge (Roy et al., 2015; Fang et al., 2016; Zeng et al., 2018). Chemical-enhanced washing, chemical adsorption/precipitation, electrokinetic extraction, and phytoremediation are effective methods for soil remediation, however, the financial and environmental constraints restrict their large-scale application (Jiang et al., 2015, Rajapaksha et al., 2016, Beiyuan et al., 2017, Wang et al., 2017).

Stabilization/solidification (S/S) is a time- and cost-efficient technology for soil remediation, and ordinary Portland cement (OPC) is a proven agent for S/S, owing to its low cost, universal applicability, and good workability (Xu et al., 2015; Benassi et al., 2016; Wang et al., 2018b). Potentially toxic elements can be effectively immobilized in the OPC-based matrix by the mechanisms of physical encapsulation and chemical fixation (Liu et al., 2018; Shao et al., 2018). However, the

* Corresponding author.
*E-mail address:* dan.tsang@polyu.edu.hk (D.C.W. Tsang).

https://doi.org/10.1016/j.envint.2019.02.057
Received 29 November 2018; Received in revised form 14 February 2019; Accepted 21 February 2019
Available online 28 February 2019

application of cement-based S/S is associated with massive $CO_2$ emission due to the high carbon footprint of OPC production (0.66–0.82 t $CO_2$ per tonne) (Dung and Unluer, 2017; Pan et al., 2017). In addition, there are durability concerns such as decalcification, degradation, and potential leaching in view of the limited compatibility between cement and soil/clay (Provis et al., 2015; Savija and Lukovic, 2016). Although cement has an excellent immobilization efficiency for metallic elements, the sole use of cement is insufficient for immobilization of metalloid elements, especially for cases in which both metallic and metalloid elements exist simultaneously (Li et al., 2018; Wang et al., 2018c; Wang et al., 2019). Therefore, it is necessary to explore alternative, low-carbon, and high-efficiency cementitious materials for the S/S of contaminated soils containing both metallic and metalloid elements.

Supplementary cementitious materials (SCMs), such as fly ash, silica fume, and granulated blast-furnace slag, are widely used to partially replace cement, which can reduce cost and energy consumption (Gu et al., 2018; Ke et al., 2018; Kumar et al., 2018). However, the limited supply of these materials in many countries is an obstacle to their wider application (Juenger and Siddique, 2015). Sole reliance on SCMs will make it difficult to achieve sustainable development of cementitious materials (Scrivener et al., 2017). In comparison, kaolinitic clays (> 40% kaolinite) are low-cost and widely accessible materials worldwide. During calcination (700 °C), the kaolinite can undergo dihydroxylation into metakaolin (MK) (Eq. (1)) (Abdelli et al., 2017).

$$Al_2O_3(SiO_2)_2{\cdot}(H_2O)_2\ (\text{kaolinite}) \rightarrow Al_2O_3(SiO_2)_2{\cdot}(H_2O)_x\ (\text{metakaolin}) + (2-x)H_2O \quad (1)$$

Compared to OPC manufacturing, MK production has notably less $CO_2$ emission (0.175 t $CO_2$ per tonne) (Kavitha et al., 2016). The calcined clay presents high pozzolanic reactivity due to the presence of alumina- and silica-rich phases with partially disordered structures (Antoni et al., 2012). These Al and Si-rich phases in clay minerals also demonstrate excellent compatibility with soil/clay as well as metallic/metalloid elements (Mukhopadhyay et al., 2017).

Alkali (mainly lime) can activate calcined clay into hydrates via pozzolanic reaction. The clay hydration process includes three major steps, i.e., dissolution of Al/Si precursors, polymerization of Al/Si-OH species, and polycondensation and precipitation of Al/Si hydrates (Provis and Bernal, 2014). Based on ideal chemical reactions (Eqs. (2)–(4)), the dosage of lime determines the final products of clay minerals (Gameiro et al., 2012).

$$AS_2\ (s) + 6CH\ (s) + 9H\ (l) \rightarrow C_4AH_{13}\ (s) + 2CSH\ (s) \quad (2)$$

$$AS_2\ (s) + 5CH\ (s) + 3H\ (l) \rightarrow C_3AH_6\ (s) + 2CSH\ (s) \quad (3)$$

$$AS_2\ (s) + 3CH\ (s) + 6H\ (l) \rightarrow C_2ASH_8\ (s) + CSH\ (s) \quad (4)$$

MK can react with calcium hydroxide (CH), water, and sulphate to generate cementitious products, such as calcium silicate hydrate (CSH) and calcium aluminum hydrate (CAH) at ambient temperature (Bucher et al., 2017; Avet et al., 2018). These minerals, as the hydration products of calcined clay, can potentially serve as a chemical stabilizer for toxic elements. However, the chemical interactions between clay minerals and potentially toxic elements and the transformation/stability of final products should be further elucidated.

To further reduce the carbon footprint, herein limestone is considered as a potential alternative to partially replace clay minerals, in view of the substantial environmental merits associated with its worldwide abundance and the elimination of the energy-intensive sintering process from its production (Huang et al., 2018). As for the S/S products, the addition of limestone may introduce a densification effect on the paste-aggregate transition zone and a refinement effect on the hydration products via nucleation mechanisms. Moreover, limestone and calcined clay can spontaneously react in an alkaline environment (Bucher et al., 2017). The limestone can react with aluminate provided by calcined clay and CH to form carboaluminates (hemi or mono) according to Eq. (5) (Antoni et al., 2012).

$$A\ (s) + C\underline{C}\ (s) + 3CH\ (s) + H\ (l) \rightarrow C_3A{\cdot}C\underline{C}{\cdot}H_{12}\ (s) \quad (5)$$

It is thus hypothesized in this study that the *co*-addition of limestone and calcined clay can offer synergistic enhancement for polymerization of hydrates and properties of soil S/S products. To provide scientific insights for an innovative and green engineering solution, this study intends to: (i) assess the efficacy of lime and limestone for the hydration and polymerization of clay minerals; (ii) elucidate the immobilization mechanisms of As and Pb in the clay mineral systems; (iii) investigate the potential interference of As and Pb on clay hydration; and (iv) validate the environmental applicability of calcined clay for novel and sustainable S/S of contaminated soil.

## 2. Materials and methodology

### 2.1. Materials and sample preparation

The contaminated soil was collected from the top 30 cm of an agricultural field near the Tancheon mine in Gongju City, Chungcheongnam-do Province, Korea (Beiyuan et al., 2017). The field was banned for agricultural use after the detection of high contents of As (2047 mg $kg^{-1}$) and Pb (1677 mg $kg^{-1}$) in the soil. The soil sample was air-dried and passed through a 2-mm screen before use. The soil was acidic with a pH value of 4.24, and its other physiochemical properties are shown in Table S1 (Supplementary Information). The MK was obtained from Super Cnpowder Technology Company, Hunan Province, China, which was calcined from kaolinite at 700 °C. The MK was composed of 50.3% $SiO_2$ and 47.0% $Al_2O_3$, with a fine particle size (< 3.4 μm). The lime (CaO > 99.9%) was an analytical reagent from Sigma-Aldrich. The limestone (> 99% $CaCO_3$, particle size < 6.5 μm) was obtained from Yuen Technology Company, Jiangsu, China. Waste phosphogypsum (PG, with 86.7% $CaSO_4$) was incorporated in the binder system to obtain favourable rheology, whereas a polycarboxylate-based superplasticizer (SP) was added to achieve an acceptable flowability of the mixture.

In this study, based on Eq. (2)–(4), the molar ratios of MK ($Al_2O_3{\cdot}2SiO_2$) to lime (CaO) were designed at 1:1; 1:3, and 1:6, respectively. Limestone was incorporated in the mineral system at the MK to limestone ($CaCO_3$) ratio at 1:1 (Eq. (5)). According to the elemental content of the raw materials (XRF data), the molar ratios of MK, lime, and limestone were converted into their mass ratios. The dosage of PG at 6 wt% of MK, the water-to-solid ratio at 0.55, and the SP-to-solid ratio of 0.04 were used in all samples based on our preliminary experiments. The corresponding mass ratios of various mixture compositions are shown in Table 1.

For the clay mineral pastes production, superplasticizer was dissolved into water to form a homogeneous solution and subsequently poured into the pre-mixed solid materials (MK, lime, limestone and PG in all the samples, and additional $NaAsO_2$/$Pb(NO_3)_2$ reagents in As/Pb incorporated samples) with 2 min stirring. The fresh pastes were then

**Table 1**
Mixture formulations (wt%) for clay mineral pastes.

| | MK/Lime/CC molar ratio | MK | Lime | CC | PG | SP | Water | Total |
|---|---|---|---|---|---|---|---|---|
| M-L | 1:1:0 | 47.93 | 12.09 | 0.00 | 2.88 | 2.52 | 34.59 | 100.00 |
| M-3L | 1:3:0 | 34.62 | 26.20 | 0.00 | 2.08 | 2.52 | 34.59 | 100.00 |
| M-6L | 1:6:0 | 24.44 | 36.99 | 0.00 | 1.47 | 2.52 | 34.59 | 100.00 |
| M-L-C | 1:1:1 | 35.68 | 9.00 | 16.07 | 2.14 | 2.52 | 34.59 | 100.00 |
| M-3L-C | 1:3:1 | 27.74 | 20.99 | 12.50 | 1.66 | 2.52 | 34.59 | 100.00 |
| M-6L-C | 1:6:1 | 20.80 | 31.48 | 9.37 | 1.25 | 2.52 | 34.59 | 100.00 |

MK: metakaolin; CC: calcium carbonate; PG: phosphogypsum; SP: superplasticizer.

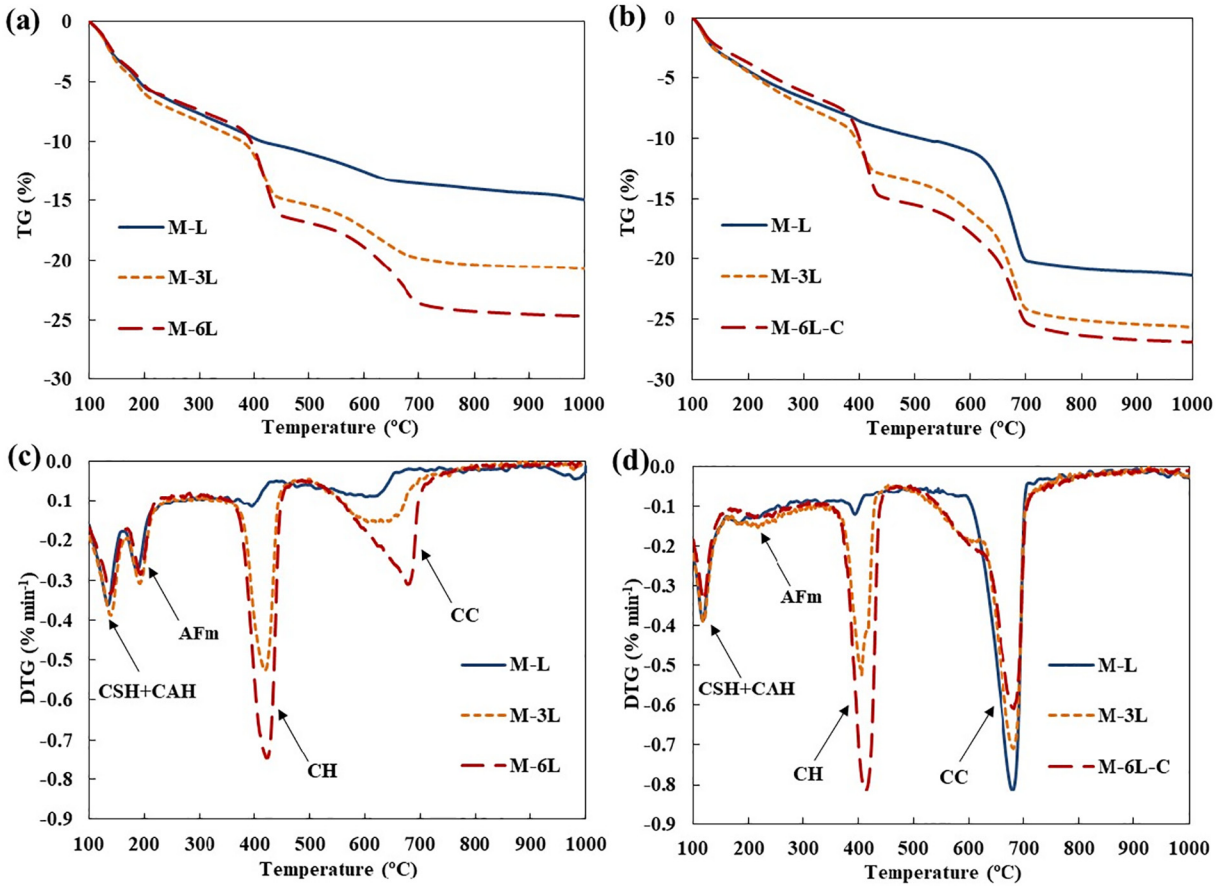


**Fig. 1.** TGA of 28-d clay mineral pastes with different dosage of lime and limestone: (a) TG curves of pastes without limestone; (b) TG curves of pastes with limestone; (c) DTG curves of pastes without limestone; (d) DTG curves of pastes with limestone. (AFm: aluminate ferrite monosulfate; CAH: calcium aluminum hydrate; CC: calcite; CH: portlandite; CSH: calcium silicate hydrate).

transferred into moulds (2 cm × 2 cm × 2 cm) and vibrated for 1 min to release the entrapped bubbles. The hardened clay mineral blocks were demoulded and enshrouded with a plastic wrap (to maintain moisture) and kept at 23 ± 1 °C for 3-d, 7-d, and 28-d air curing before assessment. For the contaminated soil S/S, the soil-to-binder mass ratio was kept at 8.5:1.5. To begin, clay mineral binders were made with the same procedure as described above. Then, well-mixed binders were poured into the wet soil (30 wt% water content) and stirred for 2 min to achieve homogenous matrix, which was filled into steel moulds (5 cm × 5 cm × 5 cm) and vibrated for 1 min. After demoulding, soil S/S blocks were enshrouded with a plastic wrap at 23 ± 1 °C for 7-d and 28-d air curing. All experiments on mineral pastes and soil S/S blocks were conducted in quadruplicate for quality assurance.

### 2.2. Spectroscopic/microscopic analyses, mechanical properties, contaminant leachability

Mineralogy of the powdered clay minerals was analysed by quantitative X-ray diffraction (Q-XRD) using a high-resolution X-ray diffractometer (Rigaku SmartLab). A 20 wt% corundum ($Al_2O_3$) as an internal admixture was added to determine the content of the amorphous phase. Samples were scanned over with a range from 5° to 35° 2θ at a rate of 2.5° $min^{-1}$ at 45 kV and 200 mA. The Rietveld refinement quantitative phase was calculated by the whole powder pattern fitting (WPPF) method available in Rigaku's integrated software (PDXL). The speciation of As in clay minerals was analysed using X-ray photoelectron spectroscopy (XPS, PHI 5000 Versaprobe II) at the Al Kα X-ray energy. A broad scan was performed with a pass energy of 187.85 eV, whereas the narrow scan of Al, Si, Ca, and As was measured with an energy of 58.7 eV. The XPS spectra were fitted by 30% Lorentzian-Gaussian function and a Shirley baseline using the program XPSPEAK41. The sub-peaks were identified with reference to the literature based on their binding energies (NIST, 2012).

The qualitative and quantitative analyses of Al-based materials were examined by a 400 MHz solid-state nuclear magnetic resonance spectrometer (NMR, Bruker Ascend 400 WB). The $^{27}Al$ magic angle spinning (MAS) NMR experiments were conducted on 79.5 MHz NMR spectrometer, collecting > 1000 scans by using a 4 mm standard bore one pulse MAS probe head, and a recycle delay of 2 s. The deconvolution of overlapped peaks in $^{27}Al$ MAS NMR spectra was carried out with Origin Pro 9.0 by applying Gaussian line model. The compound compositions of clay minerals were detected by thermogravimetric analysis (TGA, Rigaku Thermo Plus) from 100 to 1000 °C at a temperature gradient of 10 °C $min^{-1}$ with Ar stripping gas. The surface morphology and elemental composition of As and Pb contaminated samples were investigated by scanning electron microscopy with energy dispersive X-ray spectroscopy (SEM-EDX, TESCAN VEGA3 XM) and transmission electron microscopy (TEM-EDX, Oxford X-Max 80 T).

The uniaxial compressive strength of clay mineral blocks and soil S/S blocks was measured by a testing machine (Testometric CXM 500–50 KN) under an unconfined condition at a loading rate of 0.5 MPa $s^{-1}$ (Wang et al., 2019). The leachability of contaminated clay minerals and soil S/S blocks was examined by using Toxicity Characteristic Leaching Procedure (TCLP) (US EPA, 1992). The concentrations of leached elements were measured using inductively coupled plasma-atomic emission spectrometry (ICP-AES, Spectro Arcos). Potential precipitation of As and Pb compounds was modelled using Visual MINTEQ ver. 3.1.

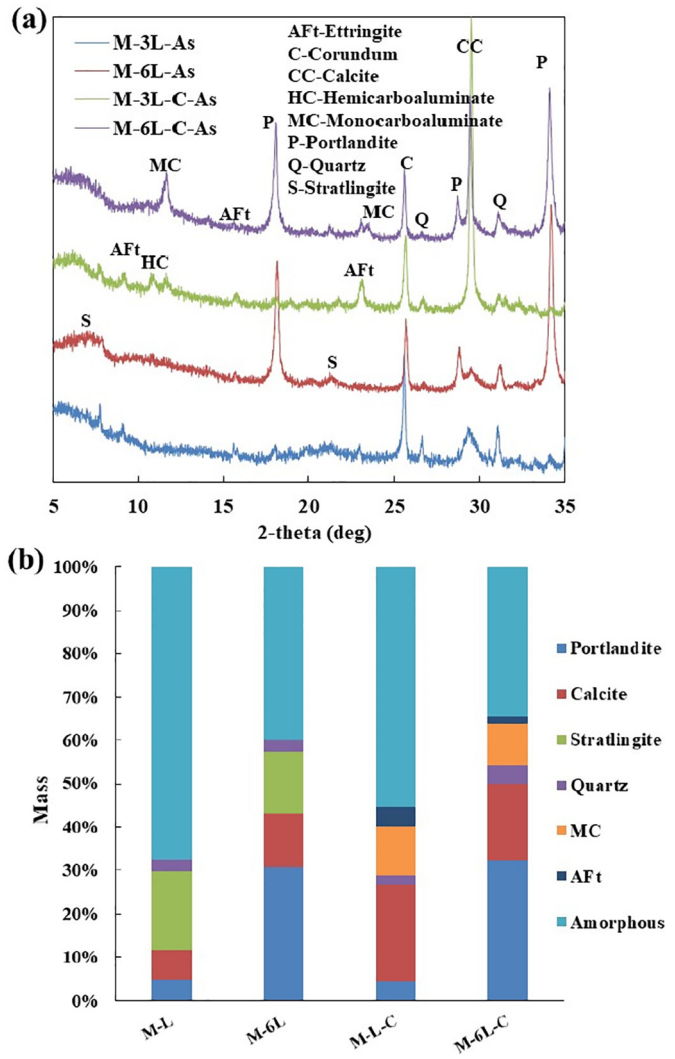


**Fig. 2.** XRD spectra (a) and Q-XRD analysis (b) of 28-d clay mineral pastes with different dosage of lime and limestone.

## 3. Results and discussion

### 3.1. Clay minerals hydration

TGA analysis was performed to elucidate the function of lime and limestone on the hydration of clay minerals. The mass loss peaks of different compositions in 28-d clay mineral pastes are illustrated in Fig. 1c and compared to the literature (Gameiro et al., 2012; Wang et al., 2018a). There were weight losses of 1.10 wt% at 420 °C and 2.14 wt% at 620 °C in the M-L samples (equivalent to 4.52 wt% Ca $(OH)_2$ and 4.86 wt% $CaCO_3$ content, respectively). Due to the indeterminacy of water removal during curing phase, the original dosage of CaO in M-L pastes should be between 12.09 wt% (based on total mass) and 19.22 wt% (based on solid mass) (Table 1). Assuming that all the lime was hydrated in the high-moisture condition, it can be calculated that only 49 to 68 wt% of CaO participated in the clay mineral formation (i.e., CSH, CAH, aluminate ferrite monosulphate (AFm), and aluminate ferrite trisulphate (AFt)).

By comparison, high-Ca samples (M-3L and M-6L) had relatively high contents of remaining CH and carbonated CC, whereas the contents of CSH, CAH, and AFm remained unchanged. This suggests that the $Ca/AS_2$ molar ratio of 1 was sufficient for activating the hydration of clay minerals, and the increase of lime dosage had an insignificant effect on hydration development. The incorporation of limestone reduced the mass loss of AFm from 2.83 wt% to 1.64 wt% (Fig. 1b). It should be noted that AFm is in general aluminate (ferrite) monosulphate phase, in which $SO_4^{2-}$ may be replaced by $OH^-$ or $CO_3^{2-}$ (Baquerizo et al., 2015). The change of mass loss reflected that the hydroxyl-rich AFm (e.g., stratlingite) may partially transform into the carbonate-rich AFm (e.g., monocarboaluminate). As the carbonate-rich AFm is more stable than the hydroxyl-rich AFm (Baquerizo et al., 2015), this transformation may be beneficial for strength enhancement of the soil S/S blocks.

The XRD spectra (Fig. 2a) confirmed that the hydroxyl-rich AFm was stratlingite (at 7.2° and 21.4°) in the limestone-free samples. The contents of stratlingite were comparable in M-L (17.8 wt%) and M-6 L (14.5 wt%) samples, although M-6 L sample had much larger content of redundant CH (31.1 wt%) (Fig. 2b), corresponding to the TGA results. This further proves that the $Ca/AS_2$ molar ratio of 1 was sufficient for activating the hydration of clay minerals. The addition of limestone resulted in the transformation of stratlingite into monocarboaluminate (MC, 18.0 wt% in M-L-C and 14.5 wt% in M-6L-C). This is further evidenced as the transformation of metastable hydroxyl-rich AFm into stable carbonate-rich AFm. In addition, the peaks of AFt (at 15.8° and 23.1°) appeared in the limestone-incorporated samples. This implies that limestone also promoted the transformation of monosulphate-rich AFm into MC, while at the same time, the released sulphate combined with remaining monosulphate-rich AFm to form AFt (aluminate trisulphate) (Antoni et al., 2012). As the unreacted MK and newly formed CSH and CAH are amorphous phase gels, which cannot be differentiated by XRD analyses, the changes of these components in different mixtures were further analysed by NMR.

The hydration products of clay minerals were characterized by $^{27}Al$ NMR (Fig. 3). As described in recent papers, two peaks of Al(III) with fourfold coordinated atoms at 70.3 ppm and 62.4 ppm account for $Al^{[IV]}$ in CSH and $Al^{[IV]}$ in AFm (i.e., stratlingite), respectively (Akhlaghi et al., 2017). The signal at 35.3 ppm can be ascribed to disordered $Al^{[V]}$ in the unreacted MK. Two peaks of $Al^{[VI]}$ in AFt and AFm are located at 9.5 ppm and 2.7 ppm, respectively (Kunther et al., 2016). $^{27}Al$ NMR results show that the majority of MK were hydrated and only 3.5 wt% of $Al^{[V]}$ remained in M-L samples. The high lime dosage in M-6 L samples slightly promoted hydration and reduced the content of $Al^{[V]}$ to 1.6 wt %, although the percentage of $Al^{[IV]}$ and $Al^{[VI]}$ were similar in two samples, corresponding to the TGA and XRD results. Furthermore, the addition of limestone significantly promoted the transformation from $Al^{[IV]}$ (tetrahedral structure) to $Al^{[VI]}$ (octahedral structure) (Alujas et al., 2015). It is possible that $CO_3^{2-}$ from limestone replaced $OH^-$ or $SO_4^{2-}$ in $Al^{[IV]}$ AFm (e.g., stratlingite) to generate octahedral $CO_3^{2-}$-rich $Al^{[VI]}$ AFm (e.g., MC). During this process, the location of the $Al^{[VI]}$ AFm peak was shifted from 2.7 ppm to −2.5 ppm. Meanwhile, the released $OH^-$ or $SO_4^{2-}$ combined with monosulphate-rich AFm to generate of AFt. As a result, in the M-L-C pastes, the $Al^{[VI]}$ phase in AFt and AFm became dominant (54.0% and 25.9%, respectively), whereas the $Al^{[IV]}$ phase was only 14% in CSH and 9% in AFm, respectively. The high polymerization ($Al^{[VI]}$) of limestone-incorporated samples may be conducive to effective solidification of the soil S/S blocks.

As shown in Fig. 4, the compressive strength of all samples increased with air curing, owing to continued hydration of clay minerals. The increasing dosage of lime had a marginal effect on the strength enhancement of limestone-free samples, which can be explained by the stable content of hydrates as revealed by the TGA, Q-XRD, and NMR results. The addition of limestone had a favourable effect on the early strength (3-d and 7-d). This can be attributed to the fact that the limestone with low water consumption increased the effective water-to-binder ratio for clay hydration; and the nature of the limestone powder may provide a filler effect for the paste matrix (Kang et al., 2018). Although the limestone addition unavoidably diluted the alkalinity of the pastes and slightly inhibited the strength development of the M-L-C pastes, the clay hydrates in the limestone-incorporated samples had a high degree of polymerization. Therefore, the high-Ca samples with

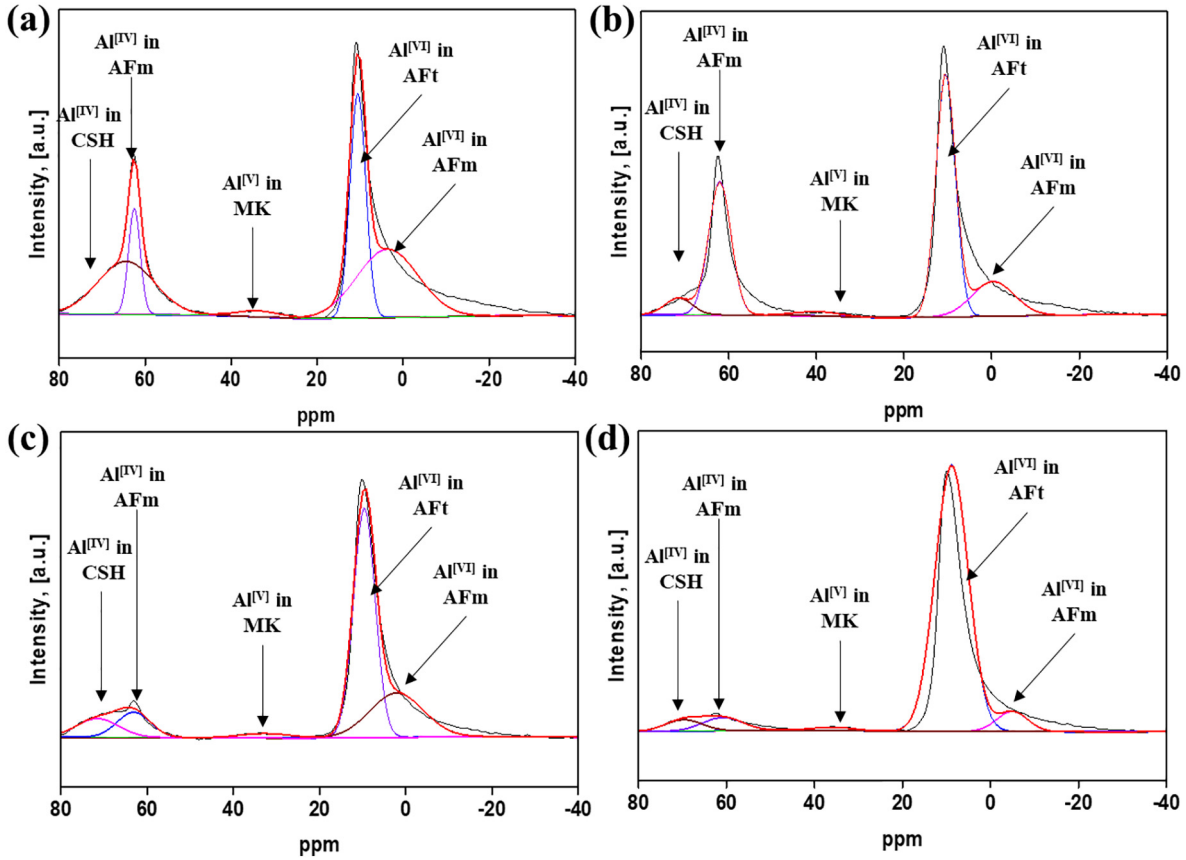


**Fig. 3.** $^{27}$Al MAS NMR spectra of 28-d clay mineral pastes with different dosage of lime and limestone: (a) M-L, (b) M-6 L, (c) M-L-C, and (d) M-6 L-C.

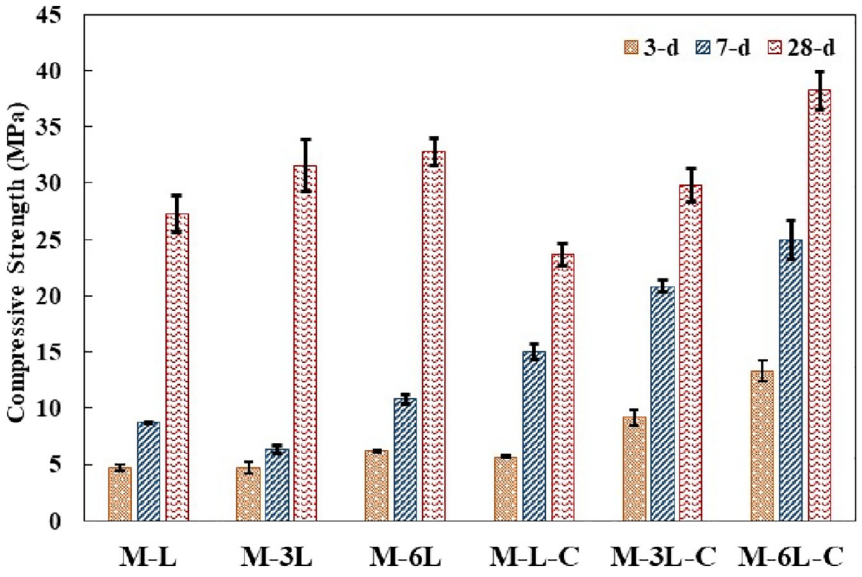


**Fig. 4.** Compressive strength of clay mineral pastes with different dosage of lime and limestone.

limestone (M-6 L-C) presented the highest 28-d compressive strength among these samples (38.2 MPa). Based on the above results, the four types of mixture (high-Ca/low-Ca, with/without limestone) were selected for the S/S of As- and Pb-contaminated soil.

### 3.2. Compatibility between clay minerals and contaminants

$^{27}$Al NMR spectra (Fig. 5) illustrated the variation of Al phases in clay minerals after the addition of As and Pb for mechanistic investigation. Compared to the M-L-C control samples, the addition of pure $NaAsO_2$ reagent resulted in the existence of abundant $Al^{[IV]}$, which is the unreacted MK (Fig. S1). This evidences that As significantly suppressed the clay hydration. By comparison, there was less unreacted $Al^{[IV]}$ in the M-L-C $Pb(NO_3)_2$-added samples. According to Visual MINTEQ modelling, the presence of limestone can provide $CO_3^{2-}$ for the precipitation of $PbCO_3$, which may reduce alkaline consumption and interference of Pb.

XPS spectra (Fig. 6a) illustrate that the dominance of As in the M-L-

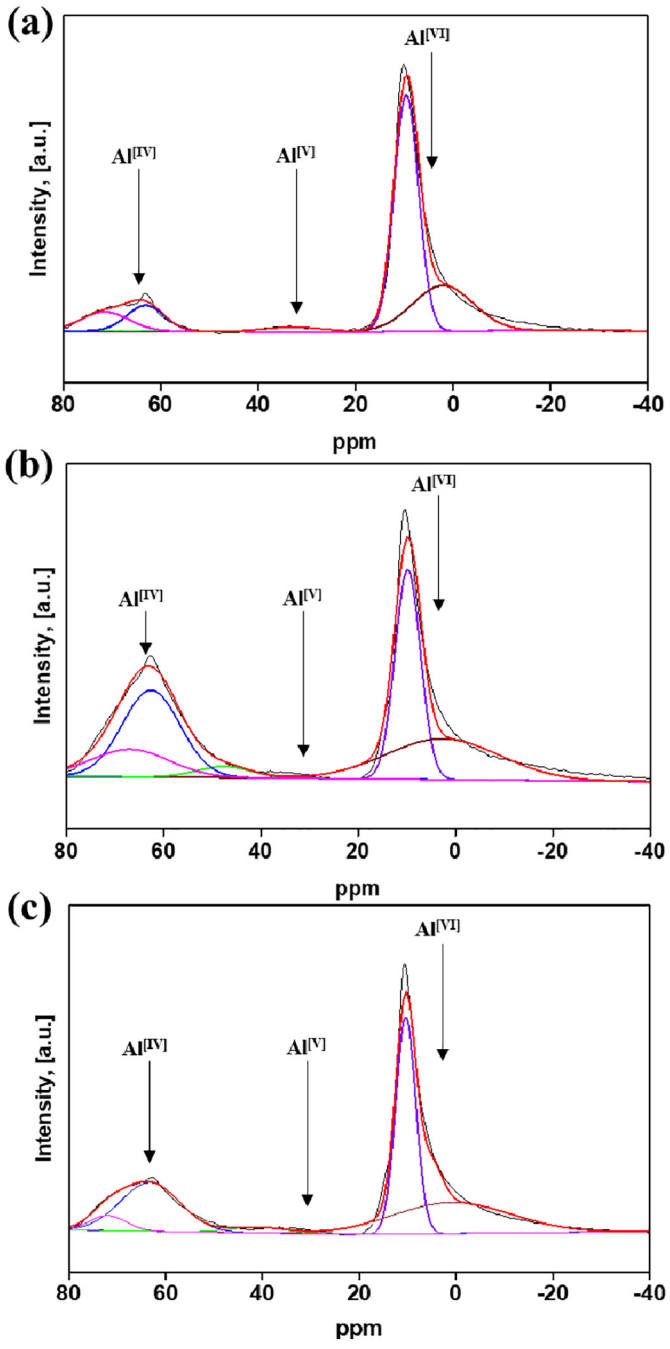


**Fig. 5.** $^{27}$Al MAS NMR spectra of 28-d clay mineral pastes with or without contaminants: (a) M-L-C paste without contaminant, (b) M-L-C paste with 20 wt % $NaAsO_2$, and (c) M-L-C paste with 20 wt% $Pb(NO_3)_2$.

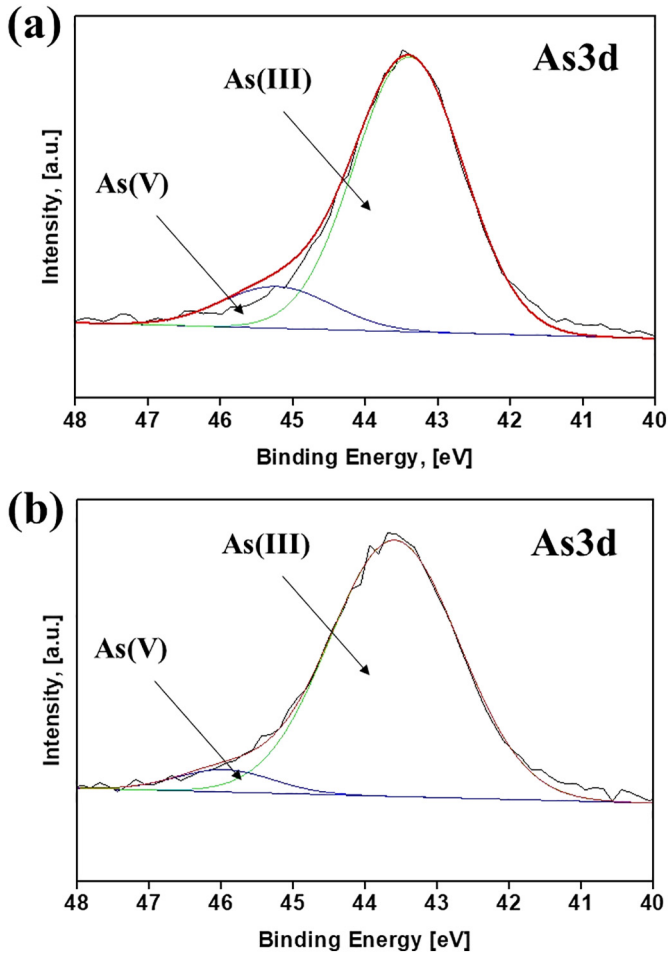


**Fig. 6.** As3d XPS spectra of 28-d clay mineral pastes containing 20 wt% $NaAsO_2$: (a) M-L-C paste with 20 wt% $NaAsO_2$; (b) M-6 L-C paste with 20 wt% $NaAsO_2$.

C samples was As(III) (at the binding energy of 43.3 eV), which was consistent with the valence state of the pure $NaAsO_2$ reagent. However, 13.2% of As appeared at the binding energy of 45.2 eV, suggesting the formation of As(V)-O (Li et al., 2018). This reflects that a part of As(III) was oxidized, which may be associated with the redox reactions promoted by clay mineral systems (Wang et al., 2014). The oxidation of As (III) to As(V) was favourable for the As immobilization, because As(V) is more stable and less toxic than As(III) (Tsang et al., 2014; Minatel et al., 2018). Compared to the M-L-C samples, the binding energies of As(V) and As(III) in M-6L-C samples were shifted to 43.6 eV and 46.0 eV, respectively. The Ca2p orbital was also shifted to higher binding energy (Fig. S2a&b). These peak shifts implied the formation of more stable Ca-As-O (Hernandez-Flores et al., 2018) in the high-Ca samples (M-6L-C) of this study. The binding energies of Al2p and Si2p were similar in the two samples (Fig. S2), indicating that Al and Si may have marginal effect on the chemical fixation of As.

The XRD patterns (Fig. S3a&b) further show that the presence of $NaAsO_2$ in the clay hydration system consumed $Ca(OH)_2$ and generated precipitates of calcium arsenate hydrates ($Ca_3(AsO_4)_2{\cdot}4H_2O$ or other forms of Ca-As-O). The reduced amount of $Ca(OH)_2$ influenced the clay hydration, because Ca is an essential element for the formation of hydrates and high alkalinity is required to activate the clay hydration (Bilondi et al., 2018). From the XRD patterns, although the degree of hydration cannot be directly determined by the change of amorphous content as unreacted MK and some clay hydrates are amorphous materials, the hydration degree can be estimated in consideration of the content variation of crystalline hydrates such as stratlingite and MC. The presence of 5 wt% $NaAsO_2$ led to the decrease of stratlingite content in the M-L (low-Ca) samples by 72.2%, whereas the decrease was only 28.7% in the M-6L (high-Ca) samples (Fig. 7a). This reflects that the hydration in low-Ca samples was severely inhibited by As, whereas high-Ca samples had better compatibility with As, because abundant Ca $(OH)_2$ can be engaged in the stable precipitation of Ca-As-O (Fig. 7b). However, the presence of 20 wt% $NaAsO_2$ consumed considerable Ca $(OH)_2$ and suppressed the formation of hydrates even in the M-6 L samples. In contrast, for the limestone-incorporated samples, the consumption of $Ca(OH)_2$ by As had an insignificant effect on the content of MC, especially in the M-6L-C samples. Because $CO_3^{2-}$ was not involved in the Ca—As precipitation, $CO_3^{2-}$ continually reacted with the hydroxyl-rich AFm to form stable MC in the clay hydration systems.

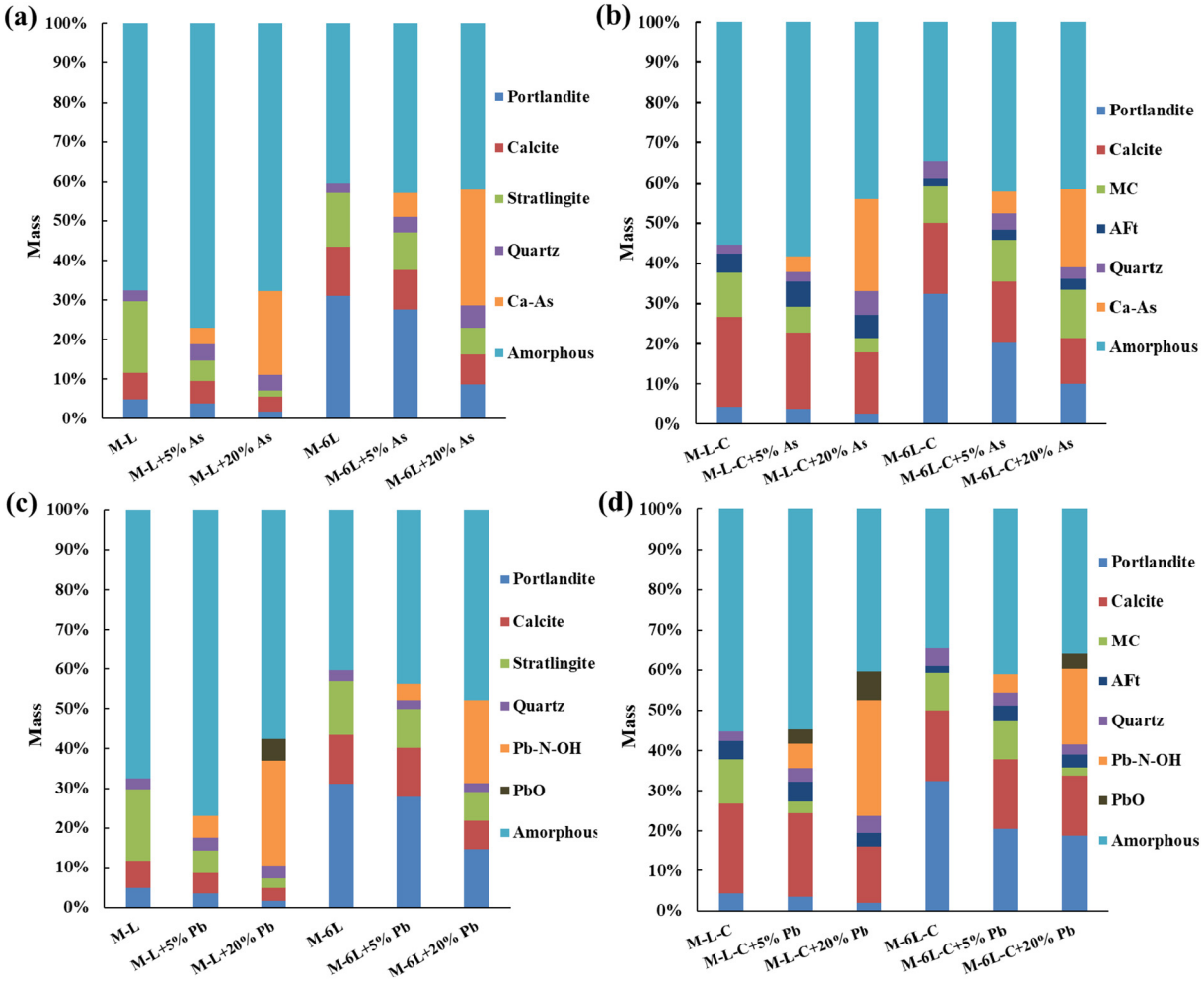


**Fig. 7.** Q-XRD analysis of 28-d clay mineral pastes with or without contaminants: (a) effect of As in clay minerals without limestone; (b) effect of As in clay minerals with limestone; (c) effect of Pb in clay minerals without limestone; (d) effect of Pb in clay minerals with limestone. (Ca-As: $Ca_3(AsO_4)_2{\cdot}4H_2O$ or $CaHAsO_3$; Pb-N-OH: $Pb(NO_3)(OH)_5$).

Therefore, $Ca(OH)_2$ was the major constituent contributing to the As precipitation and the high content of lime ($Ca/AS_2$ molar ratio of 6) was essential for activating sufficient clay hydration for the soil S/S process.

Similarly, the presence of $Pb(NO_3)_2$ reagent in the mechanistic investigation consumed $Ca(OH)_2$ and produced precipitates of $Pb_3(NO_3)(OH)_5$ (Fig. S3c&d). The Q-XRD results (Fig. 7c) show that in the M-L systems, the presence of 5 wt% $Pb(NO_3)_2$ led to the generation of $Pb_3(NO_3)(OH)_5$, whereas the stratlingite content significantly decreased by 68.9%. By comparison, Pb had a relatively small effect on the hydration of the M-6L (high-Ca) samples. In the limestone-incorporated samples, the generated $Pb_3(NO_3)(OH)_5$ may partially dehydrate to form PbO and the $CO_3^{2-}$ from limestone may react with $Pb^{2+}$ to form $PbCO_3$ (which may remain as an undetectable amorphous phase in this study), hence the MC content in the M-L-C samples decreased with increase of Pb dosage (Fig. 7d). However, in the M-6L-C (high-Ca) samples, the presence of 5 wt% $Pb(NO_3)_2$ had a marginal effect on the variation of MC content because Pb was first precipitated with $OH^-$. At 20 wt%, Pb $(NO_3)_2$ further precipitated with $CO_3^{2-}$, thereby resulting in the decreased MC formation. High content of lime ($Ca/AS_2$ molar ratio of 6) was essential in clay mineral systems for relieving the inhibitory effect of Pb on the soil S/S process.

Fig. 8a&b present typical TEM images of As and Pb contaminated clay minerals (M-L-C samples). The nanosheet morphology in Fig. 8a indicates that the As was well-blended into the clay hydrates. Dark coloured nanoparticles in the nanosheets (Fig. 8b) suggest that the Pb-compounds (mainly $Pb_3(NO_3)(OH)_5$) were physically wrapped by the clay hydrates. The Pb-compounds had a small particle size (average diameter of 2.17 nm) and were evenly distributed in the S/S matrix, further supporting the excellent compatibility between clay hydrates and contaminants (Lykhach et al., 2016). According to the elemental mapping results (Fig. 8c&d, Fig. S4a&b), As was positively correlated with Ca suggesting the precipitation of Ca and As, which was also consistent with the XRD results. However, there was a weak correlation between Pb and the other elements (Al, Si, and Ca), corroborating that Pb reacted with $Ca(OH)_2$ and generated $Pb_3(NO_3)(OH)_5$, $Pb(OH)_2$, or PbO in the soil S/S blocks.

Fig. 9a illustrates that after 5 wt% $NaAsO_2$ addition, the TCLP leaching concentrations of As in the M-L and M-L-C samples were 175.2 and 135.1 mg $L^{-1}$ (i.e., 7.0% and 5.4% in leachability), respectively. The addition of limestone had a marginal effect on the S/S performance of As-containing samples. However, increasing the lime dosage significantly enhanced the immobilization efficacy. At the $Ca/AS_2$ molar ratio of 6, the leached concentrations of As were only 0.12 mg $L^{-1}$ and 0.33 mg $L^{-1}$ in the M-L and M-L-C samples, respectively. The minimization of As leaching was attributed to the reactions with abundant $OH^-$ from lime hydration, which can react with As to generate insoluble $Ca_3(AsO_4)_2{\cdot}4H_2O$ and other forms of stable Ca-As-O. Besides, $OH^-$ could promote the generation of clay hydrates for physical encapsulation of As (Li et al., 2018). According to the Visual MINTEQ modelling, $Ca_3(AsO_4)_2{\cdot}4H_2O$ is relatively insoluble between pH 8 and 13 (Fig. S5).

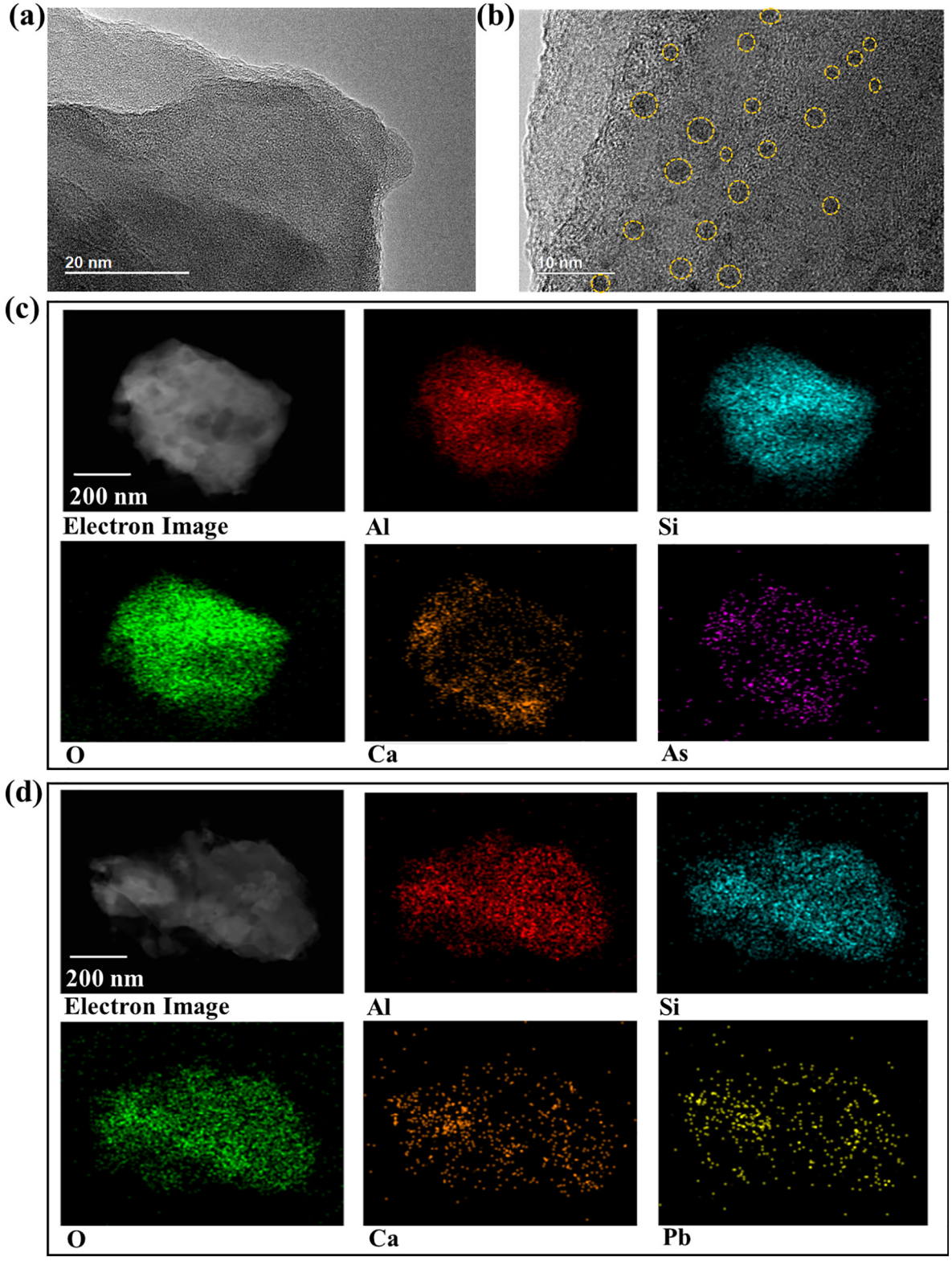


**Fig. 8.** TEM image with elemental mapping of 28-d clay mineral pastes containing As or Pb: (a) TEM image of M-L-C paste with 20 wt% $NaAsO_2$, (b) TEM image of M-L-C paste with 20 wt% $Pb(NO_3)_2$, (c) element mapping of M-L-C paste with 20 wt% $NaAsO_2$, (d) element mapping of M-L-C paste with 20 wt% $Pb(NO_3)_2$.

The $Ca_3(AsO_4)_2{\cdot}4H_2O$ was transformed into more soluble $Ca^{2+}$ and $H_2AsO^{4-}$ in the M-L and M-L-C (low-Ca) samples when the pH decreased to approximately 8 after the TCLP procedure. Regarding the Pb immobilization (Fig. 9b), the leached concentrations in the M-L and M-L-C samples were 37.6 and 34.9 mg $L^{-1}$, respectively, and the Pb leachability was further reduced in the high-Ca samples. Compared to As S/S, the effect of increasing lime dosage on Pb immobilization was relatively small. This is because $Pb(OH)_2$ and $Pb_3(NO_3)(OH)_5$ are only sparingly soluble across a wide pH range (5.5–14) (Fig. S5), these Pb components were easily precipitated in the four mixtures of clay minerals (Fig. 9b). In view of the results, the $Ca/AS_2$ molar ratio of 6 was considered suitable for effective S/S of As- and Pb-contaminated soil

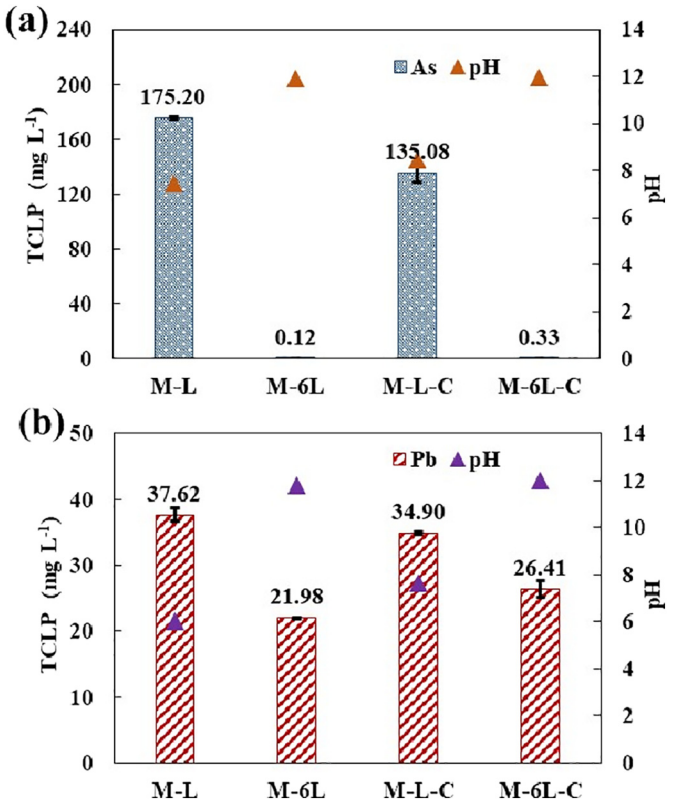


**Fig. 9.** TCLP leachability of 28-d clay mineral pastes containing As or Pb: (a) clay mineral pastes with 20 wt% $NaAsO_2$, and (b) clay mineral paste with 20 wt % $Pb(NO_3)_2$.

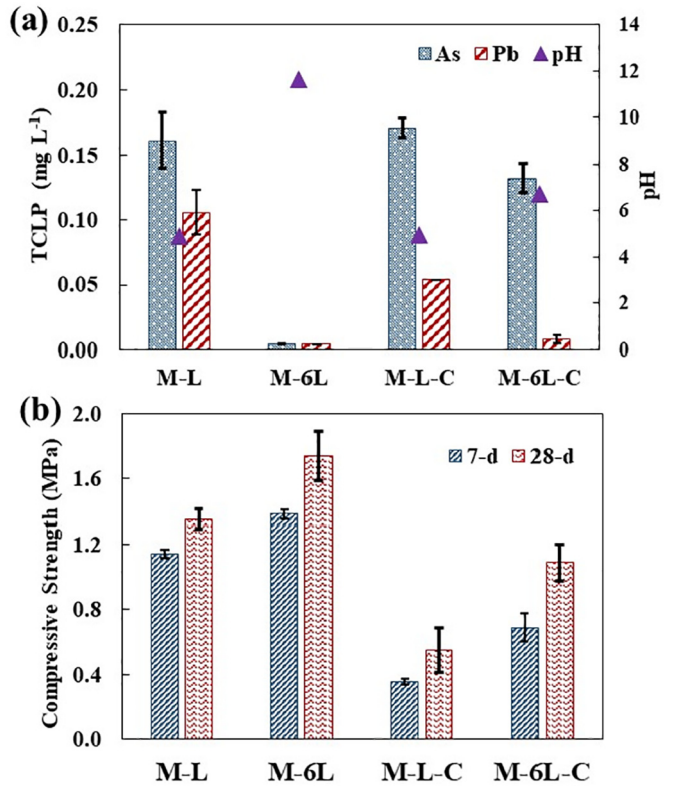


**Fig. 10.** TCLP leachability (a) and compressive strength (b) of 28-d clay-based S/S soils.

using the alkali-activated clay mineral systems.

### *3.3. Clay minerals for stabilization/solidification of As- and Pb-contaminated soil*

The TCLP results indicated that the leached concentrations of As and Pb from the contaminated soil were 1.04 ± 0.03 mg $L^{-1}$ and 3.30 ± 0.01 mg $L^{-1}$, respectively. After the clay-based S/S treatment (85 wt% soil and 15 wt% binder), the leachability of toxic elements was significantly decreased, especially in the M-6 L samples (i.e., 96.2% reduction of As and 98.8% reduction of Pb) (Fig. 10). Compared to the low-Ca samples, the high-Ca samples showed even lower leachability of As and Pb owing to abundant hydrates for chemical fixation and physical encapsulation (as revealed by NMR and Q-XRD analyses), as well as favourable pH for precipitation of toxic elements (Astrup et al., 2006; Ledesma et al., 2018). As the studied soil had a strong pH buffering capacity that hindered the pH increase even in the high-Ca samples, the leaching pH value of M-6L-C samples was only 6.7, which may need to be considered in the clay-based S/S treatment.

As shown in Fig. 10b, the 28-d compressive strength of the M-L and M-6 L samples complied with the strength requirement (1 MPa) of S/S soil as backfill materials (HK EPD, 2011). The low-Ca soil blocks were much weaker than high-Ca samples. This result corroborates that the contaminated soil with a strong pH buffering capacity consumed Ca $(OH)_2$ and impeded the alkali-activated clay hydration, especially for the low-Ca samples. The use of $CaCO_3$ led to a lower degree of hydration and lower strength, although the M-6L-C samples still fulfilled the strength requirement of 1 MPa. In view of above results, the $Ca/AS_2$ molar ratio of 6 was considered essential for effective cement-free S/S of As- and Pb-contaminated soil in this study. In future studies, biotoxicity of newly formed As and Pb phases should be assessed despite their low leachability. The change of As and Pb precipitates (i.e., durability) of the S/S soil products subjected to bioturbation and variable geochemical conditions should also be further evaluated.

## 4. Conclusions

This study investigated the roles of lime and limestone in the hydration of clay minerals and evaluated the efficacy of clay minerals for simultaneous stabilization/solidification of As and Pb in the field-contaminated soil. In the clay mineral systems, lime effectively activated the calcined clay to generate calcium silicate hydrates and calcium alumina hydrates. The addition of limestone promoted the transformation from metastable hydroxyl-rich AFm to stable carbonate-rich AFm. This process increased the degree of polymerization of clay hydrates, resulting in the enhancement of mechanical properties. The presence of As and Pb significantly interfered with the hydration of clay minerals. During the S/S process, a part of As(III) was oxidized into less toxic As(V). Both As and Pb reacted with $Ca(OH)_2$ and generated precipitates of $Ca_3(AsO_4)_2{\cdot}4H_2O$ and $Pb_3(NO_3)(OH)_5$. Due to the consumption of $Ca(OH)_2$ by As and Pb (i.e., inhibitory effects) as well as indigenous soil buffering capacity, a relatively high content of lime was essential for sufficient hydration of clay minerals in the soil S/S process. The results demonstrated that clay minerals effectively immobilized toxic elements and provided satisfactory physical encapsulation. Overall, this study presents a novel and cement-free S/S approach of As- and Pb-contaminated soil using clay minerals as low-carbon binding materials.

## Acknowledgement

The authors appreciate the financial support from the Hong Kong Research Grants Council (PolyU 15223517 and E-PolyU503/17) for this study. The authors also gratefully acknowledge the support of the University Research Facility on Chemical and Environmental Analysis (URFCE) of PolyU.

## Appendix A. Supplementary data

Supplementary data to this article can be found online at https://doi.org/10.1016/j.envint.2019.02.057.

## References


Abdelli, K., Tahlaiti, M., Belarbi, R., Oudjit, M.N., 2017. Influence of the origin of metakaolin on pozzolanic reactivity of mortars. Energy Procedia 139, 230–235.

Akhlaghi, O., Aytas, T., Tatli, B., Sezer, D., Hodaei, A., Favier, A., Scrivener, K., Menceloglu, Y.Z., Akbulut, O., 2017. Modified poly(carboxylate ether)-based superplasticizer for enhanced flowability of calcined clay-limestone-gypsum blended Portland cement. Cem. Concr. Res. 101, 114–122.

Alujas, A., Fernández, R., Quintana, R., Scrivener, K.L., Martirena, F., 2015. Pozzolanic reactivity of low grade kaolinitic clays: influence of calcination temperature and impact of calcination products on OPC hydration. Appl. Clay Sci. 108, 94–101.

Antoni, M., Rossen, J., Martirena, F., Scrivener, K., 2012. Cement substitution by a combination of metakaolin and limestone. Cem. Concr. Res. 42, 1579–1589.

Astrup, T., Dijkstra, J.J., Comans, R.N.J., Van der Sloot, H.A., Christensen, T.H., 2006. Geochemical modeling of leaching from MSWI air-pollution-control residues. Environ. Sci. Technol. 40, 3551–3557.

Avet, F., Li, X., Scrivener, K., 2018. Determination of the amount of reacted metakaolin in calcined clay blends. Cem. Concr. Res. 106, 40–48.

Baquerizo, L.G., Matschei, T., Scrivener, K.L., Saeidpour, M., Wadsö, L., 2015. Hydration states of AFm cement phases. Cem. Concr. Res. 73, 143–157.

Beiyuan, J., Awad, Y.M., Beckers, F., Tsang, D.C.W., Ok, Y.S., Rinklebe, J., 2017. Mobility and phytoavailability of As and Pb in a contaminated soil using pine sawdust biochar under systematic change of redox conditions. Chemosphere 178, 110–118.

Benassi, L., Pasquali, M., Zanoletti, A., Dalipi, R., Borgese, L., Depero, L.E., Vassura, I., Quina, M.J., Bontempi, E., 2016. Chemical stabilization of municipal solid waste incineration Fly ash without any commercial chemicals: first pilot-plant scaling up. ACS Sustain. Chem. Eng. 4, 5561–5569.

Bilondi, M.P., Toufigh, M.M., Toufigh, V., 2018. Using calcium carbide residue as an alkaline activator for glass powder-clay geopolymer. Constr. Build. Mater. 183, 417–428.

Bucher, R., Diederich, P., Escadeillas, G., Cyr, M., 2017. Service life of metakaolin-based concrete exposed to carbonation. Cem. Concr. Res. 99, 18–29.

Dung, N.T., Unluer, C., 2017. Carbonated MgO concrete with improved performance: the influence of temperature and hydration agent on hydration, carbonation and strength gain. Cem. Concr. Res. 82, 152–164.

Fang, S.E., Tsang, D.C.W., Zhou, F.S., Zhang, W.H., Qiu, R.L., 2016. Stabilization of cationic and anionic metal species in contaminated soils using sludge-derived biochar. Chemosphere 149, 263–271.

Gameiro, A.L., Silva, A.S., Veiga, M.d.R., Velosa, A.L., 2012. Lime-metakaolin hydration products: a microscopy analysis. Mater. Technol. 46, 145.

Gu, F., Peng, Z., Zhang, Y., Tang, H., Ye, L., Tian, W., Liang, G., Rao, M., Li, G., Jiang, T., 2018. Facile route for preparing refractory materials from ferronickel slag with addition of magnesia. ACS Sustain. Chem. Eng. 6, 4880–4889.

Hernandez-Flores, H., Pariona, N., Herrera-Trejo, M., Hdz-Garcia, H.M., Mtz-Enriquez, A.I., 2018. Concrete/maghemite nanocomposites as novel adsorbents for arsenic removal. J. Mol. Struct. 1171, 9–16.

HK EPD, 2011. Practice guide for investigation and remediation of contaminated land. Environmental Protection Department, Hong Kong SAR Government.

Huang, Y., Deng, M.H., Wu, S.F., Jan, J.P.G., Li, T.Q., Yang, X.E., He, Z.L., 2018. A modified receptor model for source apportionment of heavy metal pollution in soil. J. Hazard. Mater. 354, 161–169.

Jiang, N., Cai, D.Q., He, L.L., Zhong, N.Q., Wen, H., Zhang, X., Wu, Z.Y., 2015. A facile approach to remediate the microenvironment of saline – alkali soil. ACS Sustain. Chem. Eng. 3, 374–380.

Juenger, M.C.G., Siddique, R., 2015. Recent advances in understanding the role of supplementary cementitious materials in concrete. Cem. Concr. Res. 78, 71–80.

Kang, S.H., Jeong, Y., Tan, K.H., Moon, J., 2018. The use of limestone to replace physical filler of quartz powder in UHPFRC. Cem. Concr. Res. 94, 238–247.

Kavitha, O.R., Shanthi, V.M., Arulraj, G.P., Sivakumar, V.R., 2016. Microstructural studies on eco-friendly and durable self-compacting concrete blended with metakaolin. Appl. Clay Sci. 124, 143–149.

Ke, X.Y., Criado, M., Provis, J.L., Bernal, S.A., 2018. Slag-based cements that resist damage induced by carbon dioxide. ACS Sustain. Chem. Eng. 6, 5067–5075.

Kumar, N., Kupwade-Patil, K., Higuchi, R., Ferrell, D.P., Luttrull, V.A., Lynam, J.G., 2018. Use of biomass ash for development of engineered cementitious binders. ACS Sustain. Chem. Eng. 6, 13122–13130.

Kunther, W., Dai, Z., Skibsted, J., 2016. Thermodynamic modeling of hydrated white Portland cement–metakaolin–limestone blends utilizing hydration kinetics from 29 Si MAS NMR spectroscopy. Cem. Concr. Res. 86, 29–41.

Ledesma, E.F., Lozano-Lunar, A., Ayuso, J., Galvin, A.P., Fernandez, J.M., Jimenez, J.R., 2018. The role of pH on leaching of heavy metals and chlorides from electric arc furnace dust in cement-based mortars. Constr. Build. Mater. 183, 365–375.

Li, J.S., Wang, L., Cui, J.L., Poon, C.S., Beiyuan, J., Tsang, D.C.W., Li, X.D., 2018. Effects of low-alkalinity binders on stabilization/solidification of geogenic As-containing soils: spectroscopic investigation and leaching tests. Sci. Total Environ. 631-632, 1486–1494.

Liu, L.W., Li, W., Song, W.P., Guo, M.X., 2018. Remediation techniques for heavy metal-contaminated soils: principles and applicability. Sci. Total Environ. 633, 206–219.

Lykhach, Y., Kozlov, S.M., Skala, T., Tovt, A., Stetsovych, V., Tsud, N., Dvorak, F., Johanek, V., Neitzel, A., Myslivecek, J., Fabris, S., Matolin, V., Neyman, K.M., Libuda, J., 2016. Counting electrons on supported nanoparticles. Nat. Mater. 15, 284–288.

Minatel, B.C., Sage, A.P., Anderson, C., Hubaux, R., Marshall, E.A., Lam, W.L., Martinez, V.D., 2018. Environmental arsenic exposure: from genetic susceptibility to pathogenesis. Environ. Int. 112, 183–197.

Mukhopadhyay, R., Manjaiah, K.M., Datta, S.C., Yadav, R.K., Sarkar, B., 2017. Inorganically modified clay minerals: preparation, characterization, and arsenic adsorption in contaminated water and soil. Appl. Clay Sci. 147, 1–10.

NIST, 2012. NIST X-ray Photoelectron Spectroscopy Database. http://srdata.nist.gov/xps/.

Pan, S.Y., Shah, K.J., Chen, Y.H., Wang, M.H., Chiang, P.C., 2017. Deployment of accelerated carbonation using alkaline solid wastes for carbon mineralization and utilization toward a circular economy. ACS Sustain. Chem. Eng. 5, 6429–6437.

Provis, J.L., Bernal, S.A., 2014. Geopolymers and related alkali-activated materials. Annu. Rev. Mater. Res. 44, 299–327.

Provis, J.L., Palomo, A., Shi, C.J., 2015. Advances in understanding alkali-activated materials. Cem. Concr. Res. 78, 110–125.

Rajapaksha, A.U., Chen, S.S., Tsang, D.C.W., Zhang, M., Vithanage, M., Mandal, S., Gao, B., Bolan, N.S., Ok, Y.S., 2016. Engineered/designer biochar for contaminant removal/immobilization from soil and water: potential and implication of biochar modification. Chemosphere 148, 276–291.

Roy, M., Giri, A.K., Dutta, S., Mukherjee, P., 2015. Integrated phytobial remediation for sustainable management of arsenic in soil and water. Environ. Int. 75, 180–198.

Savija, B., Lukovic, M., 2016. Carbonation of cement paste: understanding, challenges, and opportunities. Constr. Build. Mater. 117, 285–301.

Scrivener, K., Martirena, F., Bishnoi, S., Maity, S., 2017. Calcined clay limestone cements (LC 3). Cem. Concr. Res. https://doi.org/10.1016/j.cemconres.2017.08.017.

Shao, N.N., Tang, S.Q., Liu, Z., Li, L., Yan, F., Liu, F., Li, S., Zhang, Z.T., 2018. Hierarchically structured calcium silicate hydrate-based nanocomposites derived from steel slag for highly efficient heavy metal removal from wastewater. ACS Sustain. Chem. Eng. https://doi.org/10.1021/acssuschemeng.8b03428.

Shi, Y.L., Chen, W.Q., Wu, S.L., Zhu, Y.G., 2017. Anthropogenic cycles of arsenic in mainland China: 1990–2010. Environ. Sci. Technol. 51, 1670–1678.

Tóth, G., Hermann, T., Silva, M.R.D., Montanarella, L., 2016. Heavy metals in agricultural soils of the European Union with implications for food safety. Environ. Int. 88, 299–309.

Tsang, D.C.W., Yip, A.C.K., Olds, W.E., Weber, P.A., 2014. Arsenic and copper stabilisation in a contaminated soil by coal fly ash and green waste compost. Environ. Sci. Pollut. Res. 21, 10194–10204.

US EPA, M, 1992. Toxicity Characteristic Leaching Procedure. U.S. Environmental Protection Agency, Washington, DC, USA.

Wang, L., Yeung, T.L.K., Tsang, D.C.W., Lau, A.Y.T., Poon, C.S., 2017. Recycling contaminated sediment into eco-friendly paving blocks by a combination of binary cement and carbon dioxide curing. J. Clean. Prod. 164, 1279–1288.

Wang, L., Chen, L., Tsang, D.C.W., Li, J.S., Baek, K., Hou, D., Ding, S., Poon, C.S., 2018a. Recycling dredged sediment into fill materials, partition blocks, and paving blocks: technical and economic assessment. J. Clean. Prod. 199, 69–76.

Wang, L., Chen, L., Tsang, D.C.W., Li, J.S., Yeung, T.L.Y., Ding, S., Poon, C.S., 2018b. Green remediation of contaminated sediment by stabilization/solidification with industrial by-products and $CO_2$ utilization. Sci. Total Environ. 631-632, 1321–1327.

Wang, L., Yu, K., Li, J.S., Tsang, D.C.W., Poon, C.S., Yoo, J.C., Baek, K., Ding, S., Hou, D., Dai, J.G., 2018c. Low-carbon and low-alkalinity stabilization/solidification of high-Pb contaminated soil. Chem. Eng. J. 351, 418–427.

Wang, L., Chen, L., Cho, D.W., Tsang, D.C.W., Yang, J., Hou, D.Y., Baek, K., Kua, H.W., Poon, C.S., 2019. Novel synergy of Si-rich minerals and reactive MgO for stabilisation/solidification of contaminated sediment. J. Hazard. Mater. 365, 695–706.

Wang, Y.H., Morin, G., Ona-Nguema, G., Brown, G.E., 2014. Arsenic(III) and arsenic(V) speciation during transformation of lepidocrocite to magnetite. Environ. Sci. Technol. 48, 14282–14290.

Xu, J., Bravo, A.G., Lagerkvist, A., Bertilsson, S., Sjöblom, R., Kumpiene, J., 2015. Sources and remediation techniques for mercury contaminated soil. Environ. Int. 74, 42–53.

Zeng, H., Yin, C., Qiao, T., Yu, Y., Zhang, J., Li, D., 2018. As(V) removal from water using a novel magnetic particle adsorbent prepared with iron-containing water treatment residuals. ACS Sustain. Chem. Eng. https://doi.org/10.1021/acssuschemeng.8b03270.

Zhao, F.J., Ma, Y.B., Zhu, Y.G., Tang, Z., McGrath, S.P., 2015. Soil contamination in China: current status and mitigation strategies. Environ. Sci. Technol. 49, 750–759.